ATMOSPHERIC ENVIRONMENT: X 30 (2026) 100446

Contents lists available at ScienceDirect

Atmospheric Environment: X

journal homepage: www.journals.elsevier.com/atmospheric-environment-x

Simulation of wake vortex transport of ultrafine particle emissions from the glide path to the ground

Frank Holzäpfel

Deutsches Zentrum für Luft- und Raumfahrt, Institut für Physik der Atmosphäre, 82234, Oberpfaffenhofen, Germany

ARTICLE INFO

Keywords:
Aviation
Ultrafine particles
Airport
Wake vortex

ABSTRACT

Ultrafine particle (UFP) emissions of aircraft may cause serious adverse health effects. The current study considers the transport of UFP emissions via the wake vortices generated by aircraft approaching Frankfurt Airport down to the ground. For this purpose, the fast-time Probabilistic Two-Phase wake vortex prediction model P2P has been enhanced for the prediction of the transport of a passive tracer with the descending wake vortex oval. The parameterisation of tracer transport considers the associated turbulent mixing processes of the vortex oval with its environment and the detrainment into a secondary wake, both causing the dilution of the tracer. The study considers the wind conditions prevailing in the year 2019 and the respective traffic mix of Frankfurt Airport. The presented results comprise the dwell times of the wake vortices reaching the ground, the corresponding passive tracer concentrations and the UFP numbers. The computed UFP numbers are set into perspective to UFP number concentrations measured at a distance of about 4 km to the airport using a mobile ground measuring station. It is found that the UFP emissions of approaching aircraft are small compared to other sources at the airport. Even UFP counts of direct wake vortex hits on the ground are on the order of the background concentrations. At a distance of 9 km from the runway ends the UFP numbers drop to less than 1% of the maximum ground immissions occurring near the runway thresholds.

1. Introduction

Besides the gaseous emissions from aircraft engines, the emitted particulate matter must also be considered. Within these ultrafine particles (UFP) smaller than 100 nm in diameter may cause serious adverse health effects, as they penetrate deep into the human respiratory system (Kreyling et al., 2006). The particulate matter emitted by jet engines of commercial aircraft are dominated by extremely fine particles, 10 to 20 nm in size (Stacey, 2019). Accordingly, jet engines of commercial aircraft may constitute a significant source of UFP in airport surroundings. Correlations between measured concentrations of particulate matter ($PM_{2.5}$, PM_{10}) and impact on health have been established from which maximum exposure limits have been derived. The WHO global air quality guidelines (2021) recommend an annual air quality guideline level for $PM_{2.5}$ of 5 $\mu g/m^3$ and a 24-h level of 15 $\mu g/m^3$. The corresponding values of the PM_{10} air quality guideline levels are 15 $\mu g/m^3$ annually and 45 $\mu g/m^3$ for 24 h. For UFP, however, the available information is insufficient to derive air quality guideline levels although risks are indicated (WHO global air quality guidelines, 2021). This study investigates to which extent the downward transport of UFP emissions by aircraft wake vortices generated during approach may contribute to the UFP exposure of communities located close to Frankfurt Airport.

There have been also a number of studies of the dispersion of tracer gases or UFP in the wakes of ground transport vehicles which are also partly controlled by coherent wake vortex structures (e.g. Carpentieri et al., 2012; Mehel and Murzyn, 2015). Several studies demonstrate that the particle size distributions of aircraft emissions can be significantly different to those caused by other emissions and may be observable for some distance downwind of the source. Harm-Altstädter et al. (2024) have investigated the vertical distributions of aircraft UFP emissions in the atmospheric boundary layer using a fixed-wing research drone about 4 km downwind of the Berlin Brandenburg Airport. They found that the degree of stability of the boundary layer strongly affects the vertical UFP profiles which generally exhibit the highest concentrations in ground proximity. Austin et al. (2021) attempted to separate UFP emissions from Seattle Tacoma Airport and road traffic using multivariate analysis based on measurements of particle size and black carbon concentrations. Emissions that could be uniquely attributed to the air traffic extended up to distances of about 4 km to the runway ends (flight height about 230 m). Ungeheuer et al. (2021) present particle-size-distribution

E-mail address: frank.holzaepfel@dlr.de.

https://doi.org/10.1016/j.aeaoa.2026.100446
Received 27 October 2025; Received in revised form 19 March 2026; Accepted 26 March 2026
Available online 2 April 2026

measurements with enhanced number concentrations of particles smaller than 50 nm during Frankfurt Airport operating hours when southwesterly winds were transporting the air masses over a four km distance from the airport to the measurement site close to Schwanheim. They further found that jet engine lubrication oils constitute excellent tracers for aircraft emissions, where the oil mass fraction is the largest in the smallest particles (Ungeheuer et al., 2022). Keuken et al. (2015) show that air traffic may contribute to elevated particle number concentrations downwind of Amsterdam Airport Schiphol even up to distances of 40 km. They identify the flight phases of take-off and climb-out as the most important particle sources followed by taxiing, waiting at the gates, and landing. Hudda and Fruin (2016) measured particle number concentrations exceeding background concentrations routinely up to downwind distances of 18 km to Los Angeles International Airport at locations under the flight tracks of landing jets (aircraft altitudes up to about 950 m). Increases in particle number concentrations could be attributed to groups of landings jets up to distances of 2.75 km to the airport. The particles measured at larger distances to the airport could not be uniquely attributed to either wake vortex transport of the emissions from the glide path down to the ground or to downwind transport of airport emissions along the glide path direction by the dominating west winds originating from the Pacific Ocean. The present study was essentially motivated by concerned residents in the vicinity of Frankfurt Airport who were unsettled by the large area in which, according to Hudda and Fruin, wake vortices can transport UFP down into populated areas.

Graham and Raper (2006a) have developed a model for the entrainment and transport of exhausts to the ground by wake vortices close to airports. Their wake vortex model predicts quite small vortex descent distances ranging from 1.5 to 2.8 wingspans corresponding to 50 m – 200 m (Graham and Raper, 2006b). By contrast, maximum descent distances of over 600 m of wake vortices generated by an A380 aircraft in cruise have been verified with a research aircraft (Brown and Holzäpfel, 2025). Graham and Raper also compared the measured and predicted ground-level concentrations of NO_x emissions at 1.2 km longitudinal distance from the runway end and found that only about 1% of NO_x was contributed by wake vortex transport. Misaka et al. (2012) have conducted Large Eddy Simulations (LES) of the transport of passive tracers by wake vortices at various conditions of environmental turbulence intensities and stable thermal stratifications, where they focused on the analysis of the turbulent exchange processes between the vortices, the vortex oval, and the environment. Unterstrasser et al. (2014) investigated wake vortex transport of aircraft emissions and the dispersion of emissions during cruise flight using LES with Lagrangian particle tracking for various environmental conditions.

The exposure of airport environments to air traffic emissions has also been modeled with comprehensive air quality simulations (Unal et al., 2005), while such investigations with air quality models typically neglect wake vortex transport of emissions towards the ground. Zhang et al. (2020) established an inventory for particle number emissions of different sources and coupled an atmospheric dispersion model with an aerosol dynamics model to quantify the aviation particle emissions from Zurich Airport. They found that the mass concentration attributable to aircraft emission was less than 1% of the annual mean concentration in most of the nearby communities while the particle number concentrations in these areas were increased by a factor of 2 to 10 compared to the background level.

The current study considers the transport of the UFP emissions by the wake vortices generated by aircraft approaching Frankfurt Airport along six different approach paths. The paper is the first to systematically investigate how large the area around an airport is in which UFP emissions from approaching aircraft can be transported to the ground by wake vortices and to classify how large this contribution could be compared to other sources at the airport. For this purpose, the fast-time Probabilistic Two-Phase wake vortex prediction model P2P has been enhanced for the prediction of the transport of a passive tracer with the descending wake vortex oval together with the associated turbulent mixing processes with its environment and the detrainment into a secondary wake, both causing the dilution of the tracer on its way to the ground. The study considers the traffic mix of Frankfurt Airport and the respective wind conditions prevailing in the year 2019. The year 2019 was selected in order to avoid adulterations of the traffic mix brought along by the COVID-19 crisis. The presented results comprise the dwell times of the wake vortices reaching the ground, the corresponding passive tracer concentrations, and UFP numbers. Finally, the computed UFP numbers are set into perspective to UFP number concentrations measured in the airport vicinity.

2. Method

2.1. Wake vortex model

The Probabilistic Two-Phase Wake Vortex Model (P2P) is a semi-empirical fast-time model, which was developed for probabilistic predictions of the transport and decay of wake vortices (Holzäpfel, 2003). Originally, the P2P model was developed for the optimization of dynamic pairwise aircraft separations on approach within a wake vortex warning system (Holzäpfel et al., 2021). It was later also applied to departures and cruise flights (Holzäpfel and Kladetzke, 2011; Sölch et al., 2016, Brown and Holzäpfel, 2025). For this purpose, the model must predict the formation, transport and decay of wake vortices quickly and reliably. To this end, P2P takes into account all relevant influencing variables of the vortex generator (wingspan, weight, speed, flight path angle) as well as the environmental parameters air density, wind (crosswind and headwind), wind shear, turbulence, thermal stratification and the influence of the ground (Holzäpfel, 2006; Holzäpfel and Steen, 2007). The model predicts both deterministic (mean) vortex development (D2P) and probabilistic envelopes with defined probabilities (P2P). P2P has been extensively validated with measurement data from over 16,000 cases from four US and ten EU measurement campaigns (Holzäpfel, 2003, 2006; Holzäpfel and Robins, 2004; Holzäpfel and Steen, 2007; Körner et al. 2017, 2019).

Fig. 1 shows an example of the development of a wake vortex near the ground measured with a 2-μm pulsed lidar system (symbols) and predicted with P2P (lines) in dimensionless variables. The vertical position z^* and the lateral position y^* of the vortex core centers are normalised with the initial vortex spacing b_0; the circulation Γ^*, which is a measure of the strength of the vortices, is normalised with its initial value, and vortex age t^*, is normalised by the time t_0 the vortices need to descend by one vortex separation b_0. The vortices generated at a height of about one vortex spacing above the ground initially descend due to mutual velocity induction before they rise again, driven by the interaction with the ground (Fig. 1a). Due to the crosswind, the vortex behaviour becomes asymmetrical and the leeward vortex rises more strongly than the windward vortex. The influence of the ground also causes the vortices to diverge, while they experience a lateral drift driven by the crosswind (Fig. 1b). P2P models the interaction with the ground by subsequently introducing image vortices and secondary vortices (Holzäpfel and Steen, 2007), where the image vortices induce the divergence of the primary vortices and the secondary vortices their subsequent rebound.

The decay of the wake vortex proceeds in two phases (Fig. 1c) and is identical for both vortices. The slower decay in the so-called diffusion phase transitions to the rapid decay phase at $t^* = 1$ due to the influence of the ground (Holzäpfel and Steen, 2007). The onset time of rapid decay is controlled by the parameter T_2^* and the decay rate by an effective viscosity ν_2^*, which are determined as a function of the energy dissipation rate of the ambient turbulence, the thermal stratification and the influence of the ground (see section 2.4). In the current study, the deterministic predictions marked with red and blue lines are used. The probabilistic envelopes, which are shown here for a 2-σ probability (95.4%), are used for conservative predictions of the vortex behaviour to

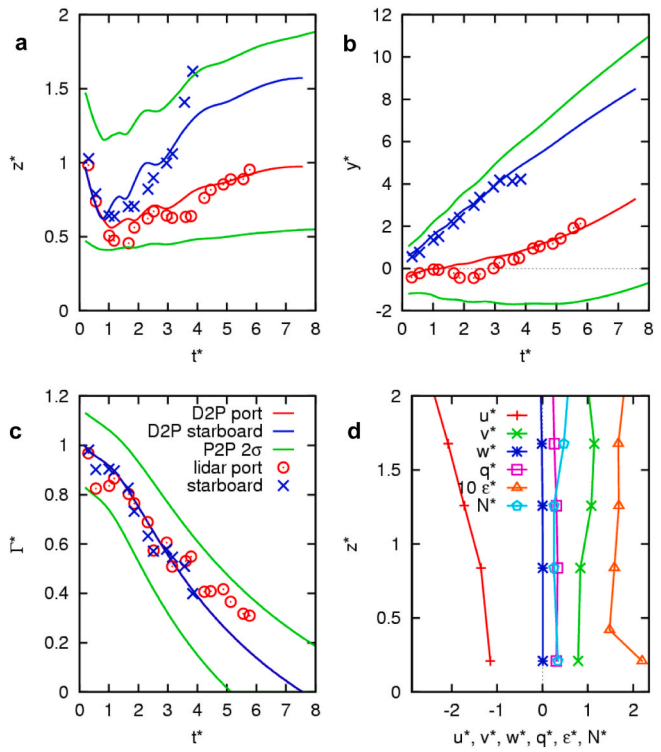

Fig. 1. Measured (symbols) and predicted (lines) wake vortex development near the ground in normalised parameters. (a) vertical position z^*, (b) lateral position y^*, and (c) vortex circulation Γ^* against vortex age t^*, (d) vertical profiles of the normalised meteorological parameters headwind u^*, crosswind v^*, vertical wind w^*, turbulence velocity q^*, turbulent kinetic energy dissipation rate ε^* (turbulence) and Brunt-Väisälä frequency N^* (thermal stratification).

adjust aircraft separations and are not used here.

In this study the energy dissipation rate of the turbulence ε, is derived from the wind speeds according to a parameterisation by Donaldson and Bilanin (1975), whereby a turbulence level of 10% is assumed. Stable thermal stratification, on the other hand, is neglected, as the width of the area that can be reached by the UFP transport is determined by strong winds, which are typically associated with weak stratification. This is a conservative assumption that tends to slightly enlarge the catchment area for the UFP transport.

2.2. Traffic data

The aircraft parameters for determining the initial circulation of the wake vortices Γ_0, and their separation b_0, are taken from the Base of Aircraft Data (BADA) database (BADA, 2019). BADA contains the data of all aircraft types used in the study. The initial vortex spacing is estimated, assuming an elliptical distribution of circulation over the wing, to $b_0 = \pi/4\ B$, where B is the wingspan. The circulation is calculated according to

$$\Gamma_0 = \frac{Mg}{\rho\pi/4BV} \tag{1}$$

from the variables aircraft mass M, gravitational acceleration g, air density ρ, wingspan B and airspeed V. Landing masses are usually treated confidentially and are only very rarely available, as they allow conclusions to be drawn about the occupancy rates of airlines. So, the weight of the approaching aircraft is adjusted following data collected at Vienna Airport, which have an average value of 90% of the maximum landing weight (Holzäpfel and Rotshteyn, 2023). Measurements at Memphis and Dallas/Fort Worth airports showed slightly lower average landing weights of 85% of the maximum landing weight (Delisi et al., 2013). According to BADA, the airspeed V, is successively reduced during the landing approach depending on the aircraft type, its mass and height above ground (Holzäpfel and Rotshteyn, 2023). The vertical profiles of the air density correspond to the International Standard Atmosphere (ISA).

Table 1 lists the considered aircraft types with the parameters relevant to this study. The analyses are carried out for air traffic and wind conditions in 2019. The number of approaches in 2019 is taken from statistics published by the airport (Frankfurt Airport Luftverkehrsstatistik, 2019). The 13 most common aircraft types account for 92.6% of aircraft movements, with the A320 family dominating with 49.6% of all approaches. Nevertheless, the proportion of aircraft in the ICAO Heavy category is relatively high at 19.9%. This is important, as the largest aircraft types also generate the longest-lived wake vortices with the greatest descent depths and therefore the largest catchment areas for UFP transport. Therefore, it is also favourable that the A380 is included in the traffic mix with a share of 1.7%. The aircraft types considered may be regarded as representative for the current purpose and are treated in the study as if they accounted for all traffic at the airport.

The airspeed, circulation and wake vortex time scale vary along an approach. The corresponding numerical values shown in Table 1 represent the final approach at altitudes below 300 m above ground. The wake vortex time scale corresponds to the time it takes for a young vortex to descend one vortex separation and scales with the lifetime of the wake vortex. The descent depth corresponds roughly to the altitude above ground at which the UFP emissions incorporated in the wake vortex can still reach the ground. This maximum descent depth or flight altitude is predicted for the longest-lived wake vortices in calm conditions without thermal stratification and without turbulence. The UFP numbers in the last column correspond to the number of non-volatile particles emitted in 1 s during the approach. They were kindly provided by the Institute of Environmental Engineering (IfU) at ETH Zurich (Zhang et al., 2019; Zhang et al., 2020). The UFP numbers for approach were taken from the ICAO-EEDB (ICAO Aircraft Engine Emissions Databank, 2023). For this purpose, the most frequent engine type of a particular aircraft type was identified via its engine Unique Identifier (UID) number provided by Frankfurt Airport. For a given engine type the fuel flow rates and the resulting non-volatile particulate matter emission indices can be found in the ICAO-EEDB.

Fig. 2 provides an overview of Frankfurt Airport with its four runways and their designations (Table 2), the location of the meteorological measuring station (HLNUG), the wind rose for 2019 (Fig. 3) and the neighbouring locations reaching up to Frankfurt am Main.

Departures are not considered as they do not contribute to the maximum extent of the area in which UFP emissions can reach the ground through wake vortex transport. According to data from German Air Traffic Control (DFS), the majority of aircraft taking off, for example of the A320 type, already reach altitudes of over 600 m at a distance of 5 km from the take-off point (Holzäpfel et al., 2009), while aircraft on approach have an altitude of only around 170 m at the same distance from the threshold (around 3 km, as the take-off point of the A320 is around 2 km from the landing threshold). Wake vortices from departures on the runway 18 West do not reach populated areas.

For the approaches to the individual runways, wake vortices are simulated starting at a distance of 12 km from the runway threshold in steps of $\Delta x = 50$ m down to the threshold, which is flown over at a height of 15 m (50 feet). This results in 240 support points per approach path for the P2P simulations. With a glide path angle of 3°, the maximum flight altitude is 643 m, whereby the individual support points for the vortex predictions have an altitude difference of 2.6 m. Table 2 shows the runway usage for landings in 2019 (Umwelt-und Nachbarschaftshaus, 2025).

The topography under the glide path is taken into account with elevation data in the WGS84 UTM Zone 32N projection, which has a resolution of 1 km x 1 km (GeoBasis-DE, 2021). For a given position of

Table 1
Aircraft types considered, sorted by number of approaches with relevant parameters (ICAO: International Civil Aviation Organization, MTOW: maximum take-off weight, MLW: maximum landing weight, WV: wake vortex).

aircraft type	ICAO weight class	approaches	MTOW [kg]	MLW [kg]	span, B [m]	airspeed, V [m/s]	circulation, Γ_0 [m^2/s]	WV-time-scale, t_0 [s]	descent distance [m]	UFP [1/s]
A320	Medium	66,489	77,000	64,500	34.1	66.9	265	17.0	205	$3.055 \cdot 10^{14}$
A321	Medium	39,678	83,000	73,500	34.1	68.6	294	15.3	205	$1.704 \cdot 10^{15}$
A319	Medium	21,272	70,000	61,000	34.1	62.7	267	16.9	205	$3.077 \cdot 10^{14}$
B737	Medium	20,124	78,300	65,310	34.3	70.5	253	18.0	208	$3.008 \cdot 10^{14}$
CRJ1-9	Medium	19,587	38,000	34,065	24.9	67.1	191	12.5	116	$1.185 \cdot 10^{12}$
E190	Medium	19,382	51,800	44,000	28.7	67.0	214	14.9	153	$2.954 \cdot 10^{14}$
B777	Heavy	12,514	299,300	237,680	60.9	73.0	500	28.8	467	$9.595 \cdot 10^{14}$
B747	Heavy	11,424	442,250	312,072	68.4	75.2	568	31.9	533	$9.674 \cdot 10^{14}$
A330	Heavy	7824	212,000	179,000	60.3	66.3	419	33.6	459	$1.401 \cdot 10^{15}$
A340	Heavy	5612	276,500	190,000	60.3	63.6	464	30.4	459	$7.812 \cdot 10^{14}$
B767	Heavy	5293	186,880	145,150	47.6	73.1	391	22.4	341	$8.158 \cdot 10^{14}$
A380	Super	4465	560,000	386,000	79.8	67.3	673	36.7	609	$6.010 \cdot 10^{15}$
B788/9/X	Heavy	4210	250,830	192,777	60.1	76.8	391	35.8	457	$9.486 \cdot 10^{14}$

Fig. 2. Overview of Frankfurt Airport with its four runways, the location of the meteorological measuring station (HLNUG), the wind rose for 2019 and the neighbouring localities including the city of Frankfurt am Main (© Google, 2026).

vortex generation, however, the terrain remains flat for vortex transport, as the P2P ground effect model does not tolerate variable elevation.

2.3. Wind conditions

A wind climatology for the year 2019 is used to compute the transport of wake vortices by the wind. For each class of wind climatology, wake vortex predictions are carried out with the respective strength and direction of the wind and the predictions are weighted with the probability of the respective wind class.

The wind data used was provided by the Hessian Agency for Nature Conservation, Environment and Geology (HLNUG). The HLNUG

Table 2
Runway utilisation for landings 2019.

runway	utilisation (%)
07R	16.1
07C	0.1
07L	15.7
25R	28.5
25C	10.0
25L	29.6

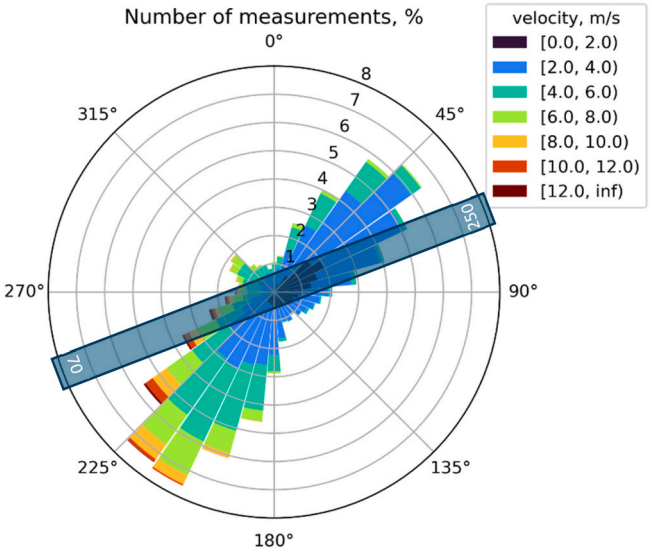

Fig. 3. Wind rose for Frankfurt Airport and the year 2019 with alignment of the runway directions of 70° and 250° (transparent blue).

weather station with the coordinates 50.04325 N 8.597167 E is installed approximately 870 m north-west of runway threshold 25L. The wind measurements are recorded at a height of 10 m by an ultrasonic anemometer and average values are available for 30 min with a discretisation of the wind speeds of 0.1 m/s and the wind directions of 1°. This data was used to create a wind climatology with 720 wind classes with a wind direction resolution of 10° and a wind speed resolution of 1 m/s. With the 240 support points for the P2P calculations along an approach, this results in 172,800 vortex predictions per runway and aircraft type.

Fig. 3 shows the resulting wind rose, in which the colour coding of the wind speed is selected in 2 m/s steps. The main wind directions of 45° and 215° are offset by around 25° to 35° to the orientations of the runways. For wind classes that exceed a tailwind of 5 kts for a given runway, approaches are typically no longer carried out, so that they are not taken into account here either. To extrapolate the wind to other heights above ground, the logarithmic wind profile is used with a ground roughness of 0.05 m, which represents a cultivated landscape with very few buildings and trees.

2.4. Parameterisation of UFP transport

Until now, the transport of emissions by wake vortices was not included in the P2P model. High-resolution Large Eddy Simulations (LES) of the transport of passive tracers by wake vortices in various environmental conditions conducted by Misaka et al. (2012) are used to parameterise the UFP transport with P2P. On the length and time scales relevant for wake vortices, it can be assumed that the UFP particles are transported in a good approximation like a passive tracer and mixed with the environment. Considering the particle Stokes number $St = \tau_p/\tau_f$, which relates the time scale of the particle relaxation to the time scale of the flow, it becomes clear that the UFP follow the fluid perfectly, since the Stokes number in the case under consideration is several orders of magnitude below one (Park and Park, 2021). So, also the simulation of a Kármán vortex street by Keita et al. (2019) illustrates that the dispersion of UFP is mainly controlled by the vortical structures and turbulent mixing in the investigated wake flow.

Firstly, the method and results of the LES by Misaka et al. (2012) are briefly recapitulated. Fig. 4 shows three different initial conditions for the distribution of the tracer in the oval bounding the air mass descending with the wake vortex. The wake vortex oval has a width of 2.09 b_0 and a height of 1.73 b_0 with a cross-sectional area of $A_{oval} = (\pi \cdot 1.73 \cdot 2.09\ b_0^2)/4$ (Greene, 1986). The two extreme assumptions that either only the vortex cores contain the tracer or that the entire oval is filled with tracer limit the spectrum of results. The initial condition, in which half the area of the oval contains the tracer, corresponds best with observations of contrail development at the end of the roll-up process of the wake vortex. The tracer concentration within the half-oval features a smooth transition from the vortex core to the half oval boundary following the magnitude of the modified stream function of the vortex pair. The parameterisation for P2P is based on this plausible mean assumption for the initial tracer distribution.

The LES elucidate that the tracer descends with the vortex oval but is also partly detrained from the oval forming a secondary wake that can extend up to the flight level (Misaka et al., 2012). Initially, the entire passive tracer descends with the wake, but at a later point in time, which depends on the environmental conditions, it is increasingly left behind in the secondary wake. It is remarkable how strongly the decrease in tracer concentration in the vortex oval correlates with the circulation decay of the wake vortices. Fig. 4 in Misaka et al. (2012) demonstrates that the half-lives for the circulation of the vortices and the concentration of the tracer almost coincide. Only in the case of very stable stratification ($N^* = 1$), which occurs only very rarely in nature, do the half-lives deviate more strongly from each other. This correlation considerably simplifies the parameterisation of tracer transport, as the dependence of vortex decay on ambient conditions has already been extensively validated and can now also be used for tracer transport.

Fig. 5 shows the normalised circulation decay of wake vortices for

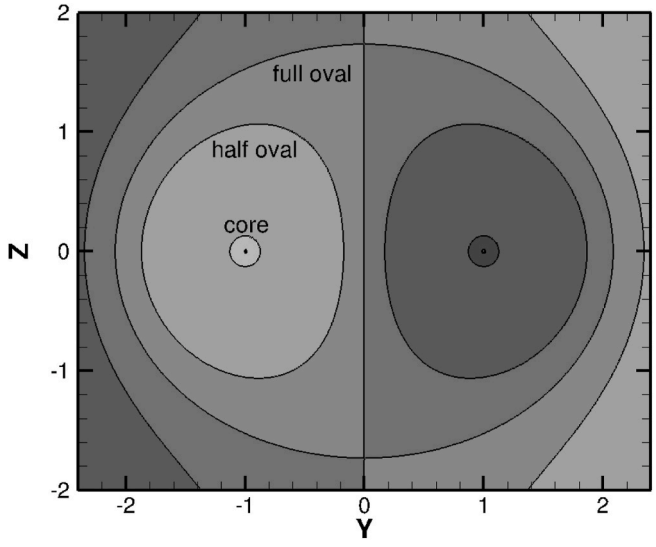

Fig. 4. Initial distributions of the tracer concentration in the vortex oval used in the LES. The unit of length corresponds to half the distance of one vortex separation b_0.

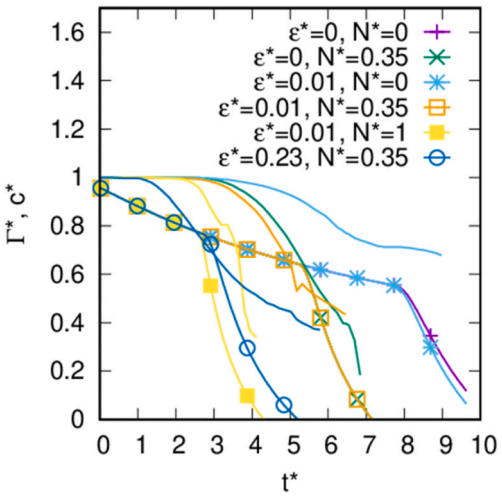

Fig. 5. Comparison of the circulation decay of P2P (lines with symbols) with the tracer concentration from the LES (lines). Normalised circulation Γ^* and tracer concentration c^* against vortex age t^* for different values of energy dissipation rate ε^* and Brunt-Väisälä frequency N^*.

different degrees of the turbulent kinetic energy dissipation rate ε^*, and the Brunt-Väisälä frequency N^*, characterizing thermal stratification as calculated with P2P (lines with symbols). In the figure lines without symbols denote the corresponding developments of the tracer concentrations in the primary wake c^*, found in the LES. This comparison illustrates the correlation between decay and tracer concentration. In particular, the correlation of the rapid decay with the rapid decrease in concentration is clearly pronounced.

Fig. 6 now compares the temporal development of the passive tracer from the LES with the parameterisation developed for the P2P model. The P2P parameterisation has four phases.

(i) The normalised tracer concentration descending with the primary wake vortex pair c^*, remains constant at the initial value of one until the time $T_{2,trac}{}^*/2$. The vortex age $T_{2,trac}{}^*$ corresponds approximately to the time of onset of rapid vortex decay $T_2{}^*$, and is determined as a function of the ambient turbulence ε^*, and thermal stratification N^* (Holzäpfel, 2003). $T_{2,trac}{}^*$ is $1.05 \cdot T_2{}^*$, which ensures a smooth progression of the concentration distribution.

(ii) Then, until $T_{2,trac}{}^*$, there is a linear decrease in the concentration from $c^* = 1$ to the value that the normalised circulation has at the time of the onset of rapid decay $c^* = \Gamma^*(T_{2,trac}{}^*)$.

(iii) The concentration then follows the rapid decay of the circulation $c^*(t^*) = \Gamma^*(t^*)$ for $t^* > T_{2,trac}{}^*$

(iv) until the tracer concentration reaches the value $c^* = 0.35$, which is maintained until the complete decay of the wake vortex ($\Gamma^* = 0$).

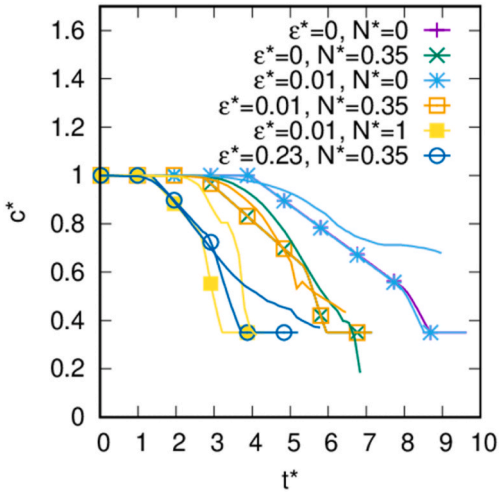

Fig. 6. Tracer concentration curve from the LES (lines) and corresponding P2P parameterisation (lines with symbols) for different environmental conditions.

The agreement between the tracer concentration curves of the LES and the P2P parameterisation is particularly good for the most frequent average weather situation at Frankfurt Airport, with weak stable stratification with a Brunt-Väisälä frequency of around $N^* = 0.35$ paired with weak atmospheric turbulence of $\varepsilon^* = 0.01$ (Frech et al., 2007).

For the calculation of the UFP transport, emission numbers of the individual aircraft types are used. These are available as non-volatile particle counts per second of flight. This means that the emissions behind the aircraft can be initialised via the airspeed as the number of particles emitted per simulated 50 m segment. These particles are transported with the wake vortices, whereby their number decreases according to the dilution caused by turbulent mixing and the detrainment into the secondary wake. Processes such as coagulation, condensation/evaporation or dry deposition are neglected.

As soon as a wake reaches the ground, the respective number of particles is assigned to the respective ground segment. A wake vortex has reached the ground when its wake vortex cores have descended below a height of $z = 0.9\ b_0$ above the ground. This corresponds to the height at which the vortex oval (see Fig. 4), which theoretically has a vertical dimension of $1.73\ b_0$ (Greene, 1986), approximately touches the ground. Note that the study only considers the UFP transport over the lifetime of the generated wake vortices. The further drift of the particles by the wind after the disintegration of the wake vortices is not considered.

2.5. UFP immissions

In order to initialise the calculation of the UFP transport, the UFP emissions from Table 1 are used. Equation (2) illustrates how the target UFP number per 50 m x 50 m segment at the ground is weighted with the various parameters.

$$UFP_{(50\,m)^2} = \sum_{j=1}^{13} \frac{number\,aircraft_j}{number\,aircraft_{tot}} \left(\sum_{k=1}^{720} prob.\,wind\,class_k \left(\sum_{ix=0}^{240} \frac{UFP}{s} \cdot \frac{50\,m}{TAS_{ix}} \right) \right) \quad (2)$$

First, the UFP emissions of an aircraft per second at true airspeed (*TAS*) are translated into emissions per 50 m segment (see Table 1). These emissions are released along the glide path at 240 support points and the transport and dilution of the UFP in space and time are calculated with the P2P model starting from each support point. These calculations are carried out for all wind classes (see Fig. 3), whereby the probabilities of the wind classes add up to one. These calculations are then performed for all aircraft types in Table 1, totalled over the number of the different aircraft types (*number aircraft*) and divided by the number of approaches ($number\ aircraft_{tot}$).

Next the UFP distributions on the ground caused by the entire traffic mix under consideration of all six runway approaches 07R, 07C, 07L, 25R, 25C, and 25L are estimated. For this purpose, equation (2) is supplemented by the runway utilisation (*RWY use*).

$$UFP_{(50\ m)^2} = \sum_{i=1}^{6} RWY\ use_i \left(\sum_{j=1}^{13} \frac{number\ a/c_j}{number\ a/c_{tot}} \left(\sum_{k=1}^{720} prob.\ wind\ class_k \left(\sum_{ix=0}^{240} \frac{UFP}{s} \cdot \frac{50\ m}{TAS_{ix}} \right) \right) \right) \quad (3)$$

All calculations are carried out for all approaches to the six runways and weighted and totalled with the frequency of the respective runway use according to Table 2. These calculations provide an overall view of the UFP emissions at Frankfurt Airport and allow the relative UFP impact under the different glide paths to be compared. However, due to the weighting of the individual glide paths with the runway utilisation, the UFP values determined do not correspond to the average immissions on the ground. For the latter, the calculations using equation (2) (see Fig. 9) can be used.

3. Results and discussions

3.1. Wake vortices and passive tracer

Fig. 7a shows the area in which the wake vortices generated by a B777 aircraft approaching runway 07R descend to a height of at least z = 0.9 b_0 above ground with the winds prevailing in the year 2019. The runway threshold lies at the origin of the coordinate system and is labelled with a + symbol. The B777 was chosen as an example because it is the most common aircraft in the category Heavy in Frankfurt.

The distribution in the figure represents the dwell times of the wake vortices at the ground in a 50 m x 50 m grid. The wake vortices are transported by the winds of all 720 wind classes and the dwell times are weighted with the respective frequency of the wind class. Dwell times from both the port and starboard vortices are summed up. The area with the longest dwell times extends along the extended runway centre line and reaches a maximum of almost 53 s. Fig. 1a illustrates that the residence time below 0.9 b_0 during the interaction of the vortices with the ground can be several characteristic time scales t_0 (cf. Table 1).

The area of wake vortex ground hits in Fig. 7a is limited to 1% of the maximum dwell time corresponding to about 0.5 s. It extends up to a distance of 7900 m from the landing threshold in the opposite direction to the approach direction. There, the flight altitude is approximately 440 m, which almost corresponds to the maximum descent depth of the B777 vortex of 467 m (see Table 1). The lateral dimensions are limited by −1070 m < y < 1170 m.

Simulations with a flat ground (not shown) reveal that the topography under the glide path has only a very small influence on the wake vortex area, so that it extends only about 200 m further to a distance of 8100 m from the runway threshold, which can be explained by the fact that the terrain slopes slightly in a south-westerly direction, while the lateral dimensions remain unchanged.

Fig. 7b shows an alternative representation of the wake vortex dwell times shown in Fig. 7a as a percentage. One hundred per cent means that a 50 m x 50 m field is hit by wake vortices on average on every approach. In fact, values far above 100% also occur, as a 50 m x 50 m area can have hits from several neighbouring support points along the glide path in which the P2P simulations are initialised in the event of headwinds or tailwinds. The percentages shown vary between 1% and 197%. With an axial extension of 7970 m, the area is only slightly longer than in Fig. 7a, but the lateral dimensions of −1400 m < y < 1720 m are significantly larger.

Fig. 7c now shows the corresponding distribution of the normalised tracer concentration c^*, on the ground. This describes the proportion of the emitted passive tracer that reaches the ground on an annual average. Obviously, the tracer concentration in a 50 m x 50 m field does not increase with the dwell time of the wake vortex or the number of hits in the field. Instead, the tracer concentration of the vortex oval is assigned to a field as soon as the vortices occur in a field below the limit height of 0.9 b_0. This appears to make sense, as the lateral dimensions of the vortex oval (see Fig. 4) and the cells of the measurement grid are of the same order of magnitude and the vortex oval extends over the full length of the cell.

In the P2P calculations, each 50 m x 50 m area is assigned the maximum concentration found during an aircraft approach in a wind class. The chosen representation thus corresponds to measurements that issue just the maximum concentration captured during an aircraft approach and do not take into account the initial increase in concentrations and their subsequent decay. As the 240 P2P calculations are initialised at distances of 50 m along the glide path for an approach in one wind class, the 50 m x 50 m fields also receive hits from axially displaced initialisation points of the P2P calculations, which are offset to the grid fields in the axial direction, in the case of headwinds or tailwinds. Nevertheless, only the maximum value per field is taken into account, regardless of where the vortex prediction was initialised. The maximum values are totalled across all wind classes being weighted with the respective probability of the wind class.

The maximum value of the tracer on the ground is 0.672, i.e. 67% of the aircraft's emissions. The area shown is again limited to one hundredth of the maximum value, that is the minimum concentration shown is 0.0067. The maximum length from the threshold is 7970 m and the maximum width resides in the range −1260 m < y < 1440 m. This means that the tracer area is only 70 m longer than the wake vortex area (Fig. 7a) and up to 270 m wider. The greater width results from the fact that the maximum concentration does not increase with the dwell times of wake vortices and is therefore relatively smaller, which also shifts the outermost 1%-contour to smaller values.

3.2. UFP immissions

The UFP immissions at the ground are estimated following the calculation method introduced in section 2.5. Apart from the initialisation of the emitted UFP numbers, the procedure is analogous to tracer transport. Accordingly, the distributions of the passive tracer (Fig. 7c) and the UFP concentrations (Fig. 8a) for runway 07R are also similar in size and shape.

Fig. 8a and b document the average UFP number distributions on the ground caused by the wake vortices of a B777 on approaches to runways 07R and 25R considering all wind conditions. For approaches to 07R, the maximum UFP number is $4.42 \cdot 10^{14}$, which corresponds to 67% of the emissions per second (per 50 m segment). The 1% area extends against the direction of flight almost up to $x = 8000$ m and in lateral direction between −1260 m and 1440 m.

The maximum extension of the UFP area (based on 1% of UFP_{max}) against the flight direction up to almost $x = 8000$ m is determined by wake vortices, which were generated in calm or very weak headwinds of up to 1 m/s. With stronger headwinds, the turbulence intensity increases, so that the now faster decaying wake vortices can no longer descent as deep. In contrast, the maximum width of the UFP area is reached with strong crosswinds. The corresponding wind speeds of 4 m/s to 8 m/s usually reach their climatological maximum value (cf. Fig. 3) if they are not capped by the tailwind criterion. With stronger tailwinds above 5 kts (2.57 m/s), approaches no longer take place.

The smallest UFP number found at the ground amounts to $1.31 \cdot 10^{11}$ or 0.3‰ of the UFP number maximum (not shown). This minimum is determined by the probability of the wind class that may transport UFP

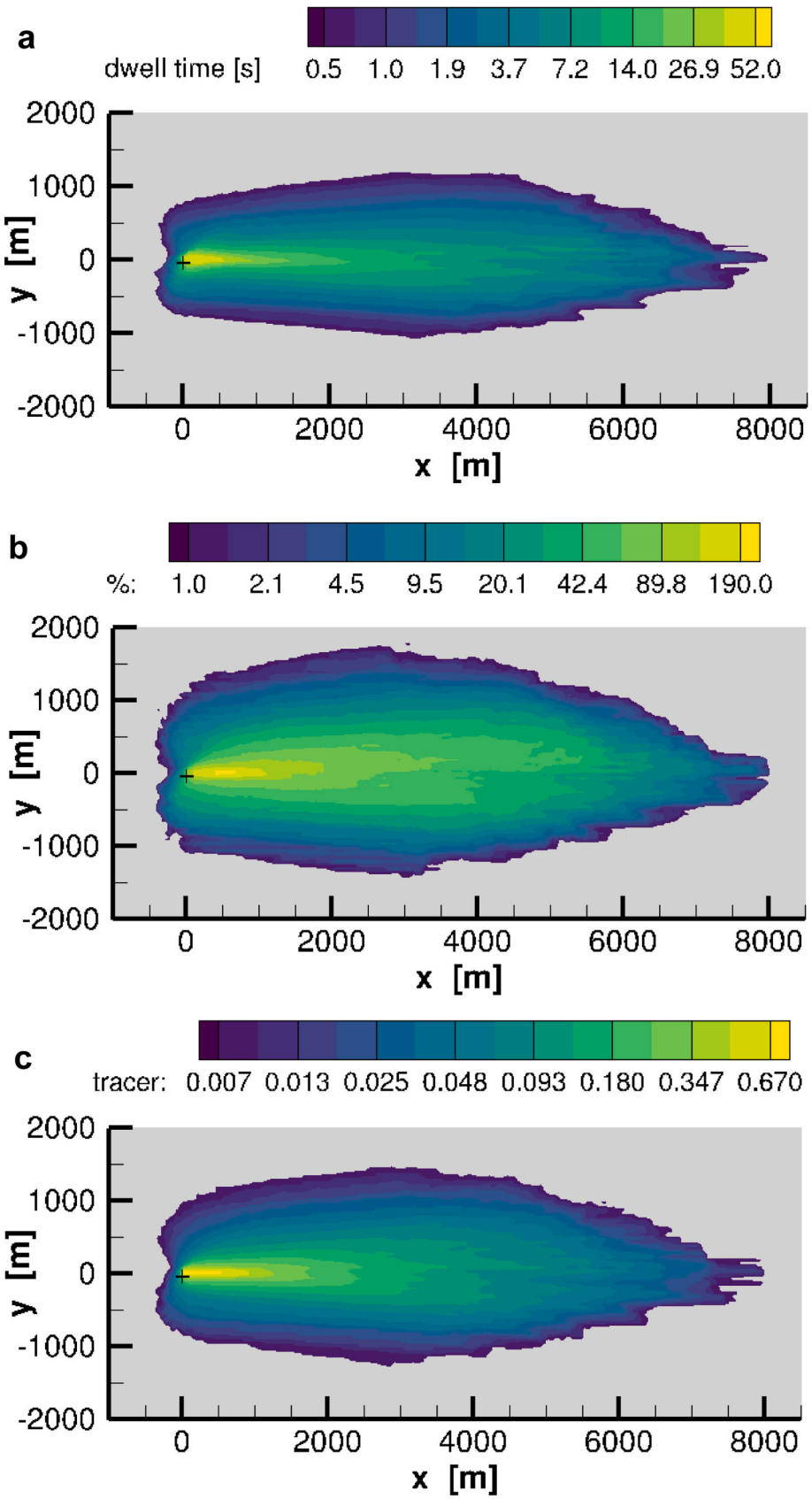

Fig. 7. Signatures of wake vortices at the ground being generated by a B777 approaching runway 07R at Frankfurt Airport. (a) dwell time at the ground; (b) percentage of vortex hits; (c) tracer distribution on the ground.

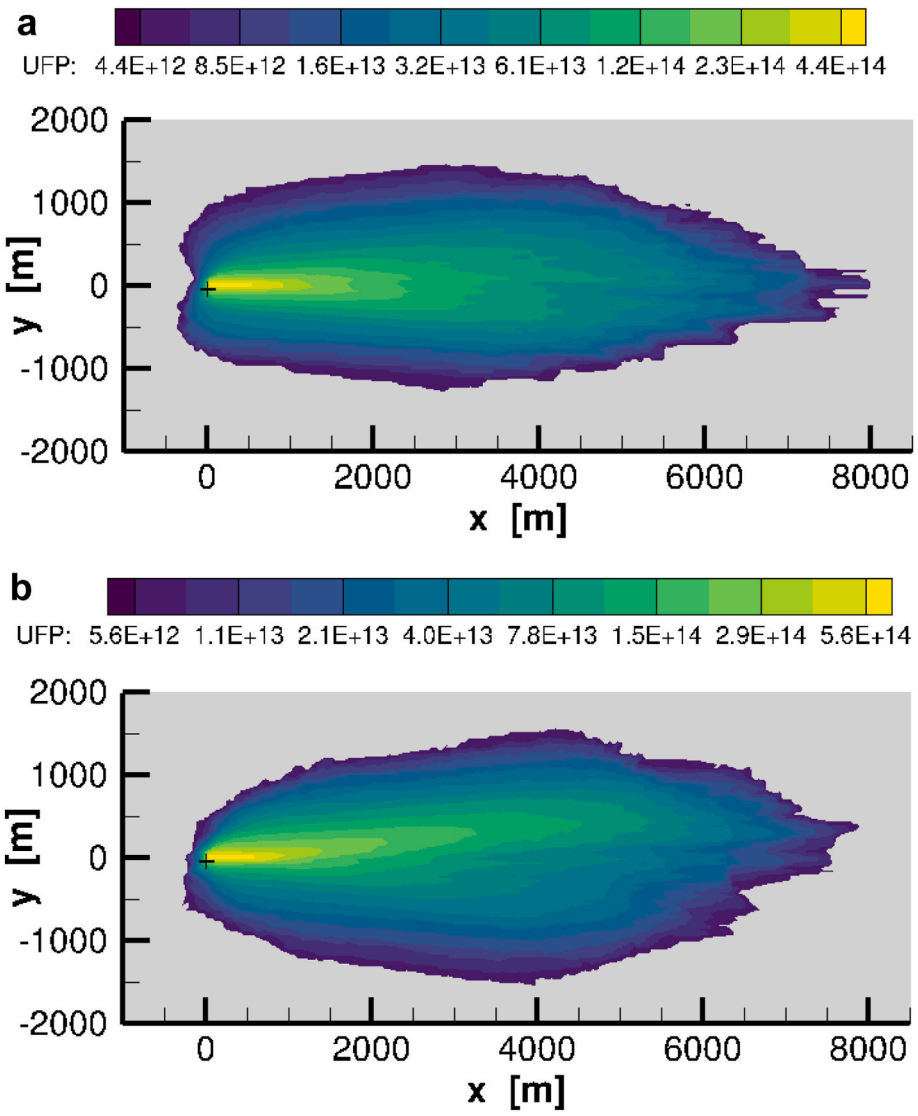

Fig. 8. UFP number distribution on the ground caused by the wake vortices of a B777 approaching (a) runway 07R and (b) runway 25R at Frankfurt Airport.

to the outermost edges of the UFP area. The corresponding absolute boundaries of the UFP area are situated against flight direction at 8425 m and the lateral extensions are −2175 m and 2325 m.

For the approach direction 25R depicted in Fig. 8b, the maximum UFP value is $5.69{\cdot}10^{14}$, which corresponds to approximately 87% of the emissions per second. The one per cent area now ends at $x = 7870$ m and lies in the lateral direction in the range $-1500\text{ m} < y < 1530$ m. This means that the areas of UFP emissions differ significantly for the two approach directions, which can be explained by the different wind conditions and the more complex terrain profile under glide path 25R.

Fig. 9 shows the UFP number distributions on the ground caused by the total traffic mix, which consists of the 13 aircraft types listed in Table 1 with their respective numbers of approaches. The result of these calculations can be interpreted as the annual mean value of the UFP count in a 50 m x 50 m field on the ground for an approach of a fictitious average aircraft according to the traffic at Frankfurt Airport with the average effect of all wind conditions. As shown in the following chapter, the calculated UFP numbers for the traffic mix under consideration can also be interpreted approximately as the UFP numbers in a cube with a side length of 50 m.

For the approaches to runway 07R shown in Fig. 9a the maximum value of the UFP number distribution of the traffic mix is $3.70{\cdot}10^{14}$ and is thus 16% smaller than the maximum of $4.42{\cdot}10^{14}$ caused by the B777. This can be explained by the relatively low UFP emissions of the highly frequent A320 family (49.6% of all approaches) which is pushing down the maximum UFP numbers close to the threshold (Table 1). The edge contour of the UFP number shown is $3.70{\cdot}10^{12}$. The length of the UFP area in the x-direction is $x = 8500$ m, which is 6% longer than the UFP area of the B777 (Fig. 8a), as the traffic mix contains the aircraft types B747 and A380 with their significantly greater wake vortex descent depths. In contrast, the lateral dimensions of $-1090\text{ m} < y < 1310$ m are 9% to 13% smaller.

Fig. 9b shows the corresponding UFP number distribution on the ground calculated for the traffic mix on approaches to runway 25R. The maximum value of $4.76{\cdot}10^{14}$ is now slightly higher, while the longitudinal extension of the area of $x = 8500$ m is the same as for the approach to runway 07R. In contrast, the lateral dimensions are slightly larger with $-1260\text{ m} < y < 1420$ m.

Next the UFP number distributions on the ground caused by the entire traffic mix along all six runway approaches are discussed. Figs. 10 and 11 show the corresponding UFP number distributions for the two approach directions. The figures are again limited to 1% of the respective maximum values. Fig. 10 shows the UFP areas for approach direction 07. As the utilisation share of runway 07C is only 1‰, the UFP distribution is largely determined by the approaches to 07R (16.1%) and 07L (15.7%). The maximum UFP number is $5.96{\cdot}10^{13}$. Fig. 10 shows

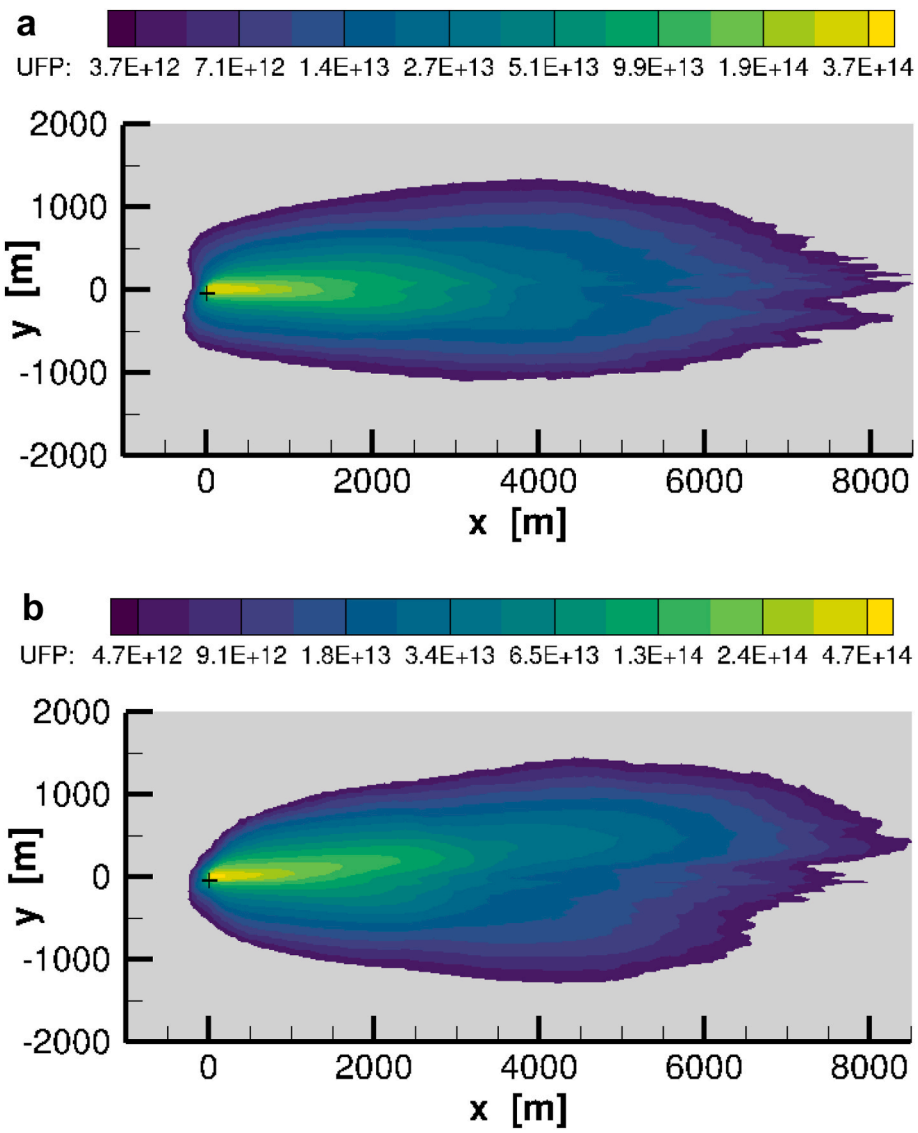

Fig. 9. UFP number distribution on the ground caused by the wake vortices of the traffic mix listed in Table 1 on approach to (a) runway 07R and (b) runway 25R at Frankfurt Airport.

UFP numbers for the towns of Rüsselsheim, Raunheim and Flörsheim, whereby the part of the development exposed to the highest UFP number is selected in each case (white + symbols). These maximum values reside between 2% and 4.5% of the maximum UFP number calculated on the ground.

Fig. 11 shows the corresponding UFP number distribution for approach direction 25. As around 68% of the approaches in 2019 took place in approach direction 25, the UFP maximum of $1.36 \cdot 10^{14}$ particles is around twice as large as for approach direction 07. As 10% of the approaches took place on the 25C, the contribution of the centre runway to the UFP distribution is now also clearly recognisable. The maximum UFP loads in the towns of Kelsterbach, Niederrad and Neu-Isenburg reside between 1% and 2% of the maximum UFP number for approach direction 25, with the towns of Kelsterbach and Niederrad both just bordering on the one per cent contour. In absolute terms, the UFP numbers in the towns of the two approach directions are similar, as two opposing effects more or less cancel each other out. On the one hand, the districts affected by approach direction 07 are significantly closer to the areas with a high UFP input, while on the other hand the air traffic is only about half as frequent.

For both approach directions, the maximum number of UFPs can be found at a distance of approximately 1 km from the landing threshold along the extended runway centre line. At a distance of approximately 9 km from the landing threshold, the UFP count has decreased to less than 1% of the maximum value on the ground. The maximum lateral distance from the extended runway centre lines amounts to about 1400 m.

3.3. *Mapping simulation results to measured UFP number concentrations*

The results of the calculations of the current study are available in the form of non-volatile UFP numbers in 50 m x 50 m fields, whereby the calculated UFP transport is weighted with the wind conditions of the entire year 2019. In Fig. 9 the calculations are weighted according to the traffic mix, while Figs. 10 and 11 also consider the runway usage. In order to be able to better evaluate these results, the calculated UFP numbers are to be set in relation to measurable UFP number concentrations (UFP number/cm^3).

Long-term measurements at the Umweltbundesamt Luftmessnetz-Zentrale in Langen, which is situated about 7 km southeasterly from Frankfurt Airport, report UFP background concentrations of 8702/cm^3 with a standard deviation of 5890/cm^3 (García-Marlès et al., 2024). At Schwanheim (mobile measurements in Fig. 11), background

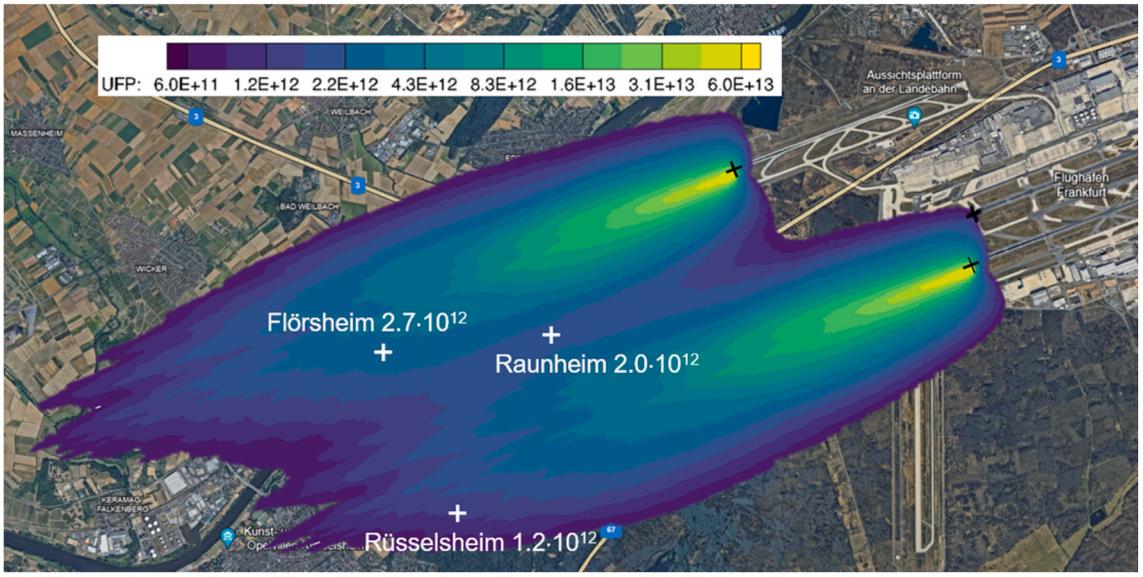

Fig. 10. UFP number distribution on the ground caused by wake vortices of the entire traffic mix in 2019 for approach direction 07 (© Google, 2024).

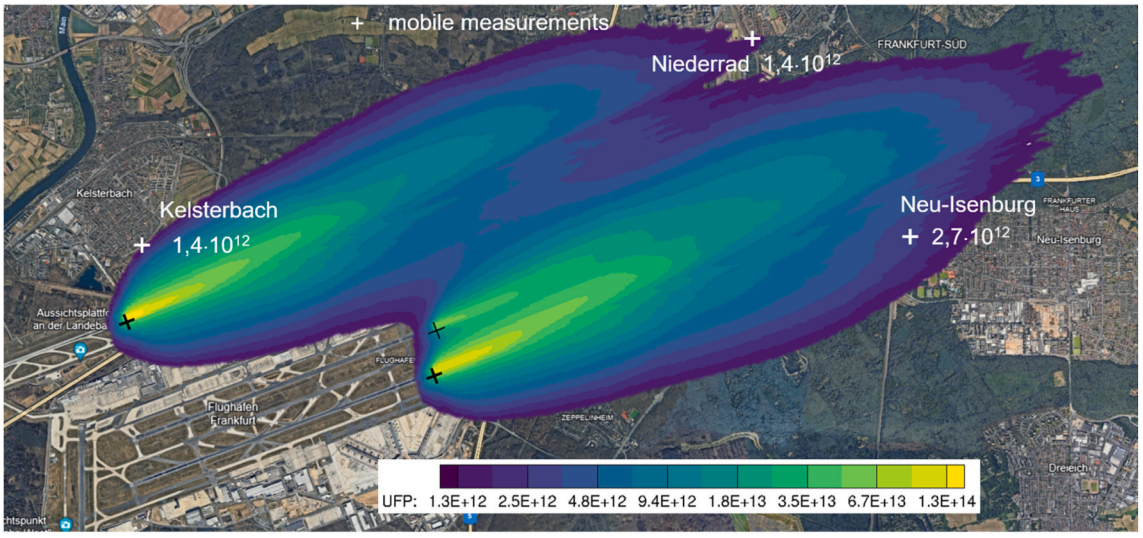

Fig. 11. UFP count distribution on the ground caused by wake vortices of the entire traffic mix in 2019 for approach direction 25. Mobile measurement site (ground and vertical measurements) as part of the SOURCE FFR measurements • modelling (© Google, 2024).

concentrations of approximately 6000/cm^3 were measured with a mobile ground measuring station (Schmitt et al., 2025), which are well within the range found in the long-term observations at Langen. In southerly winds, emissions from the airport are carried over a distance of around 4 km to the measuring station near Schwanheim, which leads to significantly increased UFP particle concentrations of around 50,000/cm^3. The ratio between volatile and non-volatile particles can be estimated at around nine for the regional UFP background (cf. Engler et al., 2007). So, the background concentration of non-volatile UFP is estimated to 670/cm^3 while the emissions advected from the airport to the UFP instrumentation amounts to about 5600/cm^3. Since the entire analysis is based on a constant ratio of volatile and non-volatile particles of nine to one, the percentage contribution from wake vortices would not change even if the total number of particles was analysed.

Next, an average volume of the descending vortex oval is estimated for the traffic mix at Frankfurt Airport. A mean vortex spacing $b_{0.mean}$ of 30.7 m can be derived from the traffic mix. The corresponding vortex oval then has a cross-section of $A_{oval,\ mean} = (\pi \cdot 1.73 \cdot 2.09\ b_{0,mean}^2)/4 =$ 2676 m^2 (Greene, 1986). At the grid length of 50 m, the mean vortex oval therefore has a volume of $V_{oval,\ mean,50m} = 133{,}800$ m^3 $= 1.34{\cdot}10^{11}$ cm^3. If it is assumed alternatively that the volume of the computational grid would be cube-shaped and therefore 50 m high, a grid element has a volume of $V_{mesh,50m} = (50\ \text{m})^3 = 125{,}000\ \text{m}^3 = 1.25{\cdot}10^{11}\ \text{cm}^3$. This means that the volumes of the average vortex oval and the computational grid are approximately the same.

Now the UFP number for approaches to runway 07R with the entire traffic mix (see Fig. 9a) along the edge contour of $3.70{\cdot}10^{12}$ can be converted to around 28/cm^3 to 30/cm^3 via the size of the computational grid or vortex oval, respectively. For runway 25R with the UFP boundary contour of $4.76{\cdot}10^{12}$ (Figs. 9b), 36/cm^3 to 38/cm^3 are obtained. So, the UFP number concentration of non-volatile particles contributed by wake vortex transport close to the mobile measurements site of less than 36 to 38/cm^3, amounts to less than 6% of the background concentration of non-volatile particles determined to 670/cm^3.

Furthermore, one may estimate what UFP concentration would be expected if the wake vortex of a selected aircraft type were to hit a

measuring point on the ground directly. Firstly, the most frequently landing aircraft type A320 is considered. According to Table 1, the A320 emits UFP/s = $3.055 \cdot 10^{14}$, which at a flight speed of 66.9 m/s is translated into a UFP number along a 50 m flight path of UFP/50m = $2.28 \cdot 10^{14}$. The vortex oval of the A320 with a cross-sectional area of A_{oval} = 2037 m^2 has a volume of $V_{oval,50m}$ = 101,850 m^3 = $1.02 \cdot 10^{11}$ cm^3. Assuming that the UFP concentration is generally diluted to 35% of the initial concentration when it reaches the ground (see Fig. 6), this results in a UFP concentration of 784/cm^3. This means that the UFP concentration is only about 1.2 times the measured background concentration of approximately 670/cm^3, even in the case of a wake vortex hit of an A320. A wake vortex hit thus corresponds to around 14% of the measured values in Schwanheim in a southerly wind with direct input of non-volatile particles from the airport (50,000/cm^3/9 = 5560/cm^3).

The wake vortex of the A380 has the largest dimensions, the longest lifetime and the deepest descent distance and is therefore most likely to reach the areas with the maximum distance from the runway threshold. The emissions of the A380 of UFP/s = $6.01 \cdot 10^{15}$ with a flight speed of 67.3 m/s result in an emission of UFP/50m = $4.47 \cdot 10^{15}$ per 50 m flight path. The vortex oval has a cross-section of A_{oval} = 11,155 m^2 and a volume of $V_{oval,50m}$ = 557,750 m^3 = $5.58 \cdot 10^{11}$ cm^3. Diluting the UFP to 35% results in a UFP concentration of 2805/cm^3, which is approximately four times the background concentration of 670/cm^3. Even this highest estimated value for the UFP input from wake vortices corresponds to only around 50% of the measured values in Schwanheim, as determined there in a southerly wind with direct particle input from the airport.

But how can the relatively small contribution of wake vortex transport to the UFP concentration on the ground be explained? Zhang et al. (2020) show in their Fig. 4 that the share of approaching aircraft in the total emissions in the vicinity of Zurich Airport is less than 3%. The proportion of taxiing, on the other hand, is over 60%. Assuming that the respective shares at Frankfurt Airport are of a similar order of magnitude, it follows that the contribution of UFP transport by wake vortices is relatively low, because the emissions during the approach are already very small. In contrast, emissions close to the ground (APU (auxiliary power unit), taxiing, take-off run, landing run) clearly dominate the contributions to the UFP, which can be transported to Schwanheim and measured under corresponding wind conditions.

4. Summary

In order to assess the contribution of the UFP transport by wake vortices to the ground, the wake vortices generated during approaches to Frankfurt Airport in 2019 were simulated. The P2P wake vortex model used for this purpose was extended to include a parameterisation of the transport of a passive tracer by the wake vortex. Processes such as coagulation, condensation/evaporation or dry deposition are neglected. The study only considers the UFP transport over the lifetime of the wake vortices generated. The further drift of the particles by the wind is not considered.

To illustrate the main mechanisms, first the dwell times of the wake vortices reaching down to the ground, as well as the passive tracer, and the UFP concentrations were presented and discussed for a B777 as an exemplary large wake vortex generator. The further calculations were based on the traffic mix at Frankfurt Airport in 2019. The results of these calculations can be interpreted as the mean values of the UFP numbers in a 50 m x 50 m mesh on the ground for approaches of a fictitious average aircraft according to the traffic at Frankfurt Airport with the average effect of all wind conditions within one annual cycle.

The maximum UFP numbers are found up to a distance of about 1 km from the threshold directly under the glide path. At a distance of approximately 9 km from the landing threshold (along the extended centre line of the respective runway), the UFP numbers have dropped to less than one per cent of their maximum value on the ground, which corresponds to less than 6% of the background number concentration of non-volatile particles measured at about 4 km distance to the airport. The maximum lateral extension of the area with UFP numbers of at least one per cent of the maximum value extends up to a distance of 1400 m from the extended centre lines of the runways. The maximum exposure of some localities in the approach area was determined as an example (Flörsheim < 0.05 UFP_{max}, Rüsselsheim < 0.02 UFP_{max}, Raunheim < 0.03 UFP_{max}, Neu-Isenburg < 0.02 UFP_{max}, Kelsterbach < 0.01 UFP_{max}, Niederrad < 0.01 UFP_{max}).

Compared to a background concentration of non-volatile particles of around 670/cm^3 measured near Schwanheim, the climatological average UFP input at the edge of the areas shown is very low at less than 40/cm^3. In the event of a direct wake vortex hit, the UFP count ranges from the background concentration value up to four times its value, depending on the aircraft type. If the wind transports the ground-level emissions of the airport directly to an area over a distance of around 4 km, UFP inputs from direct wake turbulence hits would correspond to only 14% (A320) and up to 50% (A380) of the ambient load.

The contribution of UFP transport by wake vortices appears relatively small compared to the background concentration and in particular to the ground-level emissions from the airport. This is primarily due to the fact that the emissions during the landing approach are already comparatively small and only amount to less than 3% of the airport's ground-level emissions (APU, taxiing, take-off run, landing run). Another reason is that wake vortices only reach many areas (which are not under the glide path) under certain wind conditions and direct wake vortex hits in these areas are therefore rare.

The current study confirms the findings of Zhang et al. (2020) who suggested that the contribution of UFP emissions of aircraft approaches is very small compared to other sources at an airport which comprise APU, taxiing, take-off runs, and landing runs. The maximum distance from the runway ends of about 11,500 m, where wake vortices may descend down to the ground, will be reached by the wake vortices generated by an A380 aircraft under weakly stably stratified and low turbulence conditions (Brown and Holzäpfel, 2025). Even such rare events of 600 m wake vortex descents will contribute UFP immissions which are only a few times higher than the background concentrations found in regions like Frankfurt. This makes clear that particle number concentration increases reported at distances of 18 km (Hudda and Fruin, 2016) or even 40 km (Keuken et al., 2015) from airports cannot be attributed to downward transport of wake vortices but must be caused by the advection of the emissions from the airport itself.

Declaration of competing interest

The authors declare that they have no known competing financial interests or personal relationships that could have appeared to influence the work reported in this paper.

Acknowledgements

The study SOURCE FFR measurements • modelling was funded by the Umwelthaus GmbH, a wholly-owned subsidiary of the state of Hessen and office of the Forum Flughafen und Region (FFR). The provision of the non-volatile particle emission numbers of the considered aircraft types by the Institute of Environmental Engineering (IfU) at ETH Zurich is greatly acknowledged. The instructive discussions with Markus Hermann (Leibniz-Institut für Troposphärenforschung) and Steffen Schmitt (Institut für Verbrennungstechnik, DLR) are highly appreciated.

Data availability

Data will be made available on request.

References

Austin, E., Xiang, J., Gould, T.R., Shirai, J.H., Yun, S., Yost, M.G., Larson, T.V., Seto, E., 2021. Distinct ultrafine particle profiles associated with aircraft and roadway traffic. Environ. Sci. Technol. 55, 2847–2858. https://doi.org/10.1021/acs.est.0c05933.

BADA, 2019. User Manual for the Base of Aircraft Data (BADA) Revision 3.13. EUROCONTROL, p. 119. EEC Technical/Scientific Report No. 19/03/18-45.

Brown, A.P., Holzäpfel, F., 2025. Case studies in modelling cruise-generated trailing vortices. J. Aircraft. https://doi.org/10.2514/1.C038627 article in advance.

Carpentieri, M., Kumar, P., Robins, A., 2012. Wind tunnel measurements for dispersion modelling of vehicle wakes. Atmos. Environ. 62, 9–25. https://doi.org/10.1016/j.atmosenv.2012.08.019.

Delisi, D.P., Pruis, M.J., Wang, F.Y., Lai, D.Y., 2013. Estimates of the initial vortex separation distance, b_0, of commercial aircraft from pulsed lidar data. In: 51st AIAA Aerospace Sciences Meeting Including the New Horizons Forum and Aerospace Exposition. AIAA Paper 2013-0365. https://doi.org/10.2514/6.2013-365.

Donaldson, C., Bilanin, A., 1975. Vortex wakes of conventional aircraft. AGARD Tech. Rep. 204, 79.

EEDB, 2024. ICAO aircraft engine emissions databank. Host. European Union Aviat. Safety Agen. (EASA). https://www.easa.europa.eu/en/domains/environment/icao-aircraft-engine-emissions-databank. (Accessed 23 October 2025).

Engler, C., Rose, D., Wehner, B., Wiedensohler, A., Brüggemann, E., Gnauk, Z., Spindler, G., Tuch, T, Birmili, W., 2007. Size distributions of non-volatile particle residuals (Dp < 800 nm) at a rural site in Germany and relation to air mass origin. Atmos. Chem. Phys. 7, 5785–5802. https://doi.org/10.5194/acp-7-5785-2007.

Frankfurt Airport Luftverkehrsstatistik, 2019. Fraport AG (UEW-MF). https://www.fraport.com/content/dam/fraport-company/documents/investoren/finanz–und-verkehrszahlen/luftverkehrsstatistik/luftverkehrsstatistik_2019.pdf/_jcr_content/renditions/original.media_file.download_attachment.file/luftverkehrsstatistik_2019.pdf. (Accessed 23 October 2025).

Frech, M., Holzäpfel, F., Tafferner, A., Gerz, T., 2007. High-resolution weather data base for the terminal area of frankfurt airport. J. Appl. Meteorol. Climatol. 46, 1913–1932. https://doi.org/10.1175/2007JAMC1513.1.

García-Marlès, M., Trecehera, P., Liu, X., Petäjä, T., Harrison, R., Hopke, P., Wiedensohler, A., Alastuey, A., Querol, X., 2024. Research Infrastructures Services Reinforcing Air Quality Monitoring Capacities in European Urban & Industrial Areas, Env_Guidance-Document_ST1_UFP_Definitive.pdf. (Accessed 23 October 2025).

GeoBasis-DE, 2021. Digitales Geländemodell Gitterweite 1000 m DGM1000, Geodaten der deutschen Landesvermessung, Bundesamt für Kartographie und Geodäsie, 17.03.2021. https://gdz.bkg.bund.de/index.php/default/digitales-gelandemodell-gitterweite-1000-m-dgm1000.html.

Graham, A., Raper, D.W., 2006a. Transport to ground of emissions in aircraft wakes. Part I: processes. Atmos. Environ. 40, 5574–5585. https://doi.org/10.1016/j.atmosenv.2006.05.015.

Graham, A., Raper, D.W., 2006b. Transport to ground of emissions in aircraft wakes. Part II: effect on NO_x concentrations in airport approaches. Atmos. Environ. 40, 5824–5836. https://doi.org/10.1016/j.atmosenv.2006.05.014.

Greene, G.C., 1986. An approximate model of vortex decay in the atmosphere. J. Aircraft 23, 566–573. https://doi.org/10.2514/3.45345.

Harm-Altstädter, B., Voß, A., Aust, S., Bärfuss, K., Bretschneider, L., Merkel, M., Pätzold, F., Schlerf, A., Weinhold, K., Wiedensohler, A., Winkler, U., Lampert, A., 2024. First study using a fixed-wing drone for systematic measurements of aerosol vertical distribution close to a civil airport. Front. Environ. Sci. 12, 1376980. https://doi.org/10.3389/fenvs.2024.1376980.

Holzäpfel, F., 2003. Probabilistic two-phase wake vortex decay and transport model. J. Aircraft 40, 323–331. https://doi.org/10.2514/2.3096.

Holzäpfel, F., Robins, R.E., 2004. Probabilistic two-phase aircraft wake vortex model: application and assessment. J. Aircraft 41, 1117–1126. https://doi.org/10.2514/1.2280.

Holzäpfel, F., 2006. Probabilistic two-phase aircraft wake-vortex model: further development and assessment. J. Aircraft 43, 700–708. https://doi.org/10.2514/1.16798.

Holzäpfel, F., Steen, M., 2007. Aircraft wake-vortex evolution in ground proximity: analysis and parameterization. AIAA J. 45, 218–227. https://doi.org/10.2514/1.23917.

Holzäpfel, F., Kladetzke, J., Amelsberg, S., Lenz, H., Schwarz, C., De Visscher, I., 2009. Aircraft wake vortex scenarios simulation for TakeOff and departure. J. Aircraft 46, 713–717. https://doi.org/10.2514/6.2008-8921.

Holzäpfel, F., Kladetzke, J., 2011. Assessment of wake vortex encounter probabilities for crosswind departure scenarios. J. Aircraft 48, 812–822. https://doi.org/10.2514/1.C000236.

Holzäpfel, F., Strauss, L., Schwarz, C., 2021. Assessment of dynamic pairwise wake vortex separations for approach and landing at Vienna airport. Aero. Sci. Technol. 112, 106618. https://doi.org/10.1016/j.ast.2021.106618.

Holzäpfel, F., Rotshteyn, G., 2023. Estimating aircraft landing weights from mode S data. J. Aircraft 60, 589–593. https://doi.org/10.2514/1.C036689.

Hudda, N., Fruin, S.A., 2016. International airport impacts to air quality: size and related properties of large increases in ultrafine particle number concentrations. Environ. Sci. Technol. 50, 3362–3370. https://doi.org/10.1021/acs.est.5b05313.

ICAO Aircraft Engine Emissions Databank, 2023. Introduction to the ICAO Engine Emissions Databank. EASA. https://www.easa.europa.eu/en/domains/environment/icao-aircraft-engine-emissions-databank.

Keita, N.S., Mehel, A., Murzyn, F., Taniere, A., Arcen, B., Diourte, B., 2019. Numerical study of ultrafine particles dispersion in the wake of a cylinder. Atmos. Pollut. Res. 10, 294–302. https://doi.org/10.1016/j.apr.2018.08.006.

Keuken, M.P., Moerman, M., Zandveld, P., Henzing, J.S., Hoek, G., 2015. Total and size-resolved particle number and black carbon concentrations in urban areas near Schiphol airport (the Netherlands). Atmos. Environ. 104, 132–142. https://doi.org/10.1016/j.atmosenv.2015.01.015.

Körner, S., Ahmad, N.N., Holzäpfel, F., Van Valkenburg, R.L., 2017. Multimodel ensemble methods for prediction of wake-vortex transport and decay. J. Aircraft 54, 1849–1859. https://doi.org/10.2514/1.C034287.

Körner, S., Holzäpfel, F., Sölch, I., 2019. Probabilistic multimodel ensemble wake-vortex prediction employing Bayesian model averaging. J. Aircraft 56, 695–706. https://doi.org/10.2514/1.C035109.

Kreyling, W.G., Semmler-Behnke, M., Möller, W., 2006. Health implications of nanoparticles. J. Nanopart. Res. 8, 543–562. https://doi.org/10.1007/s11051-005-9068-z.

Mehel, A., Murzyn, F., 2015. Effect of air velocity on nanoparticles dispersion in the wake of a vehicle model: wind tunnel experiments. Atmos. Pollut. Res. 6, 612–617. https://doi.org/10.5094/APR.2015.069.

Misaka, T., Holzäpfel, F., Gerz, T., Manhart, M., Schwertfirm, F., 2012. Vortex bursting, tracer transport, and decay mechanisms of a counter-rotating vortex pair. Phys. Fluids 24. https://doi.org/10.1063/1.3684990, 25104-1 - 25104-21.

Park, J., Park, H., 2021. Particle dispersion induced by vortical interactions in a particle-laden upward jet with a partial crossflow. J. Fluid Mech. 915. https://doi.org/10.1017/jfm.2021.19. A5-1 – A5-39.

Schmitt, S., Harm-Altstädter, B., Schuchard, M., Bretschneider, L., Pätzold, F., Schlerf, A., Sandgaard, J., Voß, A., Reijrink, N., Grein, T., Gaiser, N., Lampert, A., Köhler, M., 2025. Airborne and Ground Measurements of Ultrafine Particles in the Frankfurt Airport Region. GAeF START 2025, Winterthur, Schweiz.

Sölch, I., Holzäpfel, F., Abdelmoula, F., Vechtel, D., 2016. Performance of on-board wake vortex prediction systems employing various meteorological data sources. J. Aircraft 53, 1505–1516. http://arc.aiaa.org/doi/abs/10.2514/1.C033732.

Stacey, B., 2019. Measurement of ultrafine particles at airports: a review. Atmos. Environ. 198, 463–477. https://doi.org/10.1016/j.atmosenv.2018.10.041.

Umwelt- und Nachbarschaftshaus, 2021. Gemeinnützige Umwelthaus Gmbh, Kelsterbach. https://www.umwelthaus.org/fluglaerm/fluglaermmonitoring/monitoring-der-flugbewegungen/. (Accessed 23 October 2025).

Unal, A., Hu, Y., Chang, M.E., Odman, M.T., Russell, A.G., 2005. Airport related emissions and impacts on air quality: application to the Atlanta international airport. Atmos. Environ. 39, 5787–5798. https://doi.org/10.1016/j.atmosenv.2005.05.051.

Ungeheuer, F., Caudillo, L., Ditas, F., Simon, M., van Pinxteren, D., Kılıç, D., Rose, D., Jacobi, S., Kürten, A., Curtius, J., Vogel, A.L., 2022. Nucleation of jet engine oil vapours is a large source of aviation-related ultrafine particles. Commun. Earth Environ. 3, 1–8. https://doi.org/10.1038/s43247-022-00653-w.

Ungeheuer, F., van Pinxteren, D., Vogel, A.L., 2021. Identification and source attribution of organic compounds in ultrafine particles near frankfurt international airport. Atmos. Chem. Phys. 21, 3763–3775. https://doi.org/10.5194/acp-21-3763-2021.

Unterstrasser, S., Paoli, R., Sölch, I., Kühnlein, C., Gerz, T., 2014. Dimension of aircraft exhaust plumes at cruise conditions: effect of wake vortices. Atmos. Chem. Phys. 14, 2713–2733. https://doi.org/10.5194/acp-14-2713-2014.

WHO global air quality guidelines, 2021. Particulate Matter (PM2.5 and PM10), Ozone, Nitrogen Dioxide, Sulfur Dioxide and Carbon Monoxide. World Health Organization, Geneva. https://www.who.int/publications/i/item/9789240034228. (Accessed 23 October 2025).

Zhang, X., Chen, X., Wang, J., 2019. A number-based inventory of size-resolved black carbon particle emissions by global civil aviation. Nat. Commun. 10, 534. https://doi.org/10.1038/s41467-019-08491-9.

Zhang, X., Karl, M., Zhang, L., Wang, J., 2020. Influence of aviation emission on the particle number concentration near Zurich airport. Environ. Sci. Technol. 54, 14161–14171. https://doi.org/10.1021/acs.est.0c02249.